THE JOURNAL OF BIOLOGICAL CHEMISTRY VOL. 290, NO. 52, pp. 30750–30761, December 25, 2015

Asn-150 of Murine Erythroid 5-Aminolevulinate Synthase Modulates the Catalytic Balance between the Rates of the Reversible Reaction*

Received for publication, March 27, 2015, and in revised form, October 27, 2015 Published, JBC Papers in Press, October 28, 2015, DOI 10.1074/jbc.M115.655399

Bosko M. Stojanovski[‡] **and Gloria C. Ferreira**[‡§1]

From the [‡]*Department of Molecular Medicine, Morsani College of Medicine, and the* [§]*Department of Chemistry, University of South Florida, Tampa, Florida 33612*

Background: 5-Aminolevulinate synthase (ALAS) catalyzes the initial step of mammalian heme biosynthesis.
Results: N150H and N150F mutations significantly reduced the rate of quinonoid intermediate formation in the forward direction, while increasing the reverse reaction rate.
Conclusion: Asn-150 is essential for establishing a catalytic balance between the forward and reverse reactions.
Significance: This is the first report of an ALAS region modulating the ALA synthesis-breakdown balance.

5-Aminolevulinate synthase (ALAS) catalyzes the first step in mammalian heme biosynthesis, the pyridoxal 5′-phosphate (PLP)-dependent and reversible reaction between glycine and succinyl-CoA to generate CoA, CO_2, and 5-aminolevulinate (ALA). Apart from coordinating the positioning of succinyl-CoA, *Rhodobacter capsulatus* ALAS Asn-85 has a proposed role in regulating the opening of an active site channel. Here, we constructed a library of murine erythroid ALAS variants with substitutions at the position occupied by the analogous bacterial asparagine, screened for ALAS function, and characterized the catalytic properties of the N150H and N150F variants. Quinonoid intermediate formation occurred with a significantly reduced rate for either the N150H- or N150F-catalyzed condensation of glycine with succinyl-CoA during a single turnover. The introduced mutations caused modifications in the ALAS active site such that the resulting variants tipped the balance between the forward- and reverse-catalyzed reactions. Although wild-type ALAS catalyzes the conversion of ALA into the quinonoid intermediate at a rate 6.3-fold slower than the formation of the same quinonoid intermediate from glycine and succinyl-CoA, the N150F variant catalyzes the forward reaction at a mere 1.2-fold faster rate than that of the reverse reaction, and the N150H variant reverses the rate values with a 1.7-fold faster rate for the reverse reaction than that for the forward reaction. We conclude that the evolutionary selection of Asn-150 was significant for optimizing the forward enzymatic reaction at the expense of the reverse, thus ensuring that ALA is predominantly available for heme biosynthesis.

5-Aminolevulinate synthase (ALAS),[2] a homodimeric, pyridoxal 5′-phosphate (PLP)-dependent enzyme, catalyzes the first and regulatory step in mammalian heme biosynthesis, which is the condensation between glycine and succinyl-CoA to generate coenzyme A (CoA), CO_2, and 5-aminolevulinate (ALA) (1, 2). The active site of ALAS, like that of other fold type I PLP-dependent enzymes (3), is located at the dimeric interface and is composed of amino acids from the individual subunits (4). Loss-of-function and gain-of-function mutations in the erythroid-specific ALAS gene (*ALAS2*) result in X-linked sideroblastic anemia (XLSA) and X-linked protoporphyria (XLPP), respectively (5–7), suggesting that the rate of ALA synthesis is a closely regulated physiological process.

The postulated reaction mechanism for the ALAS-catalyzed reaction is shown in Scheme 1. Two carbanions, termed quinonoid intermediates (with an absorption at a λ_{max} ~510 nm), are generated during the ALAS catalytic cycle for the condensation of glycine and succinyl-CoA (8–14). An initial quinonoid intermediate is formed upon removal of the pro-*R* proton from the glycine-external aldimine complex (Scheme 1, *III*) (8–10), and a second quinonoid intermediate (henceforth referred to as quinonoid intermediate II (Scheme 1, *VII*)) results from the decarboxylation of the 2-amino-3-ketoadipate condensation intermediate (11–13). The generated enol, which is in rapid equilibrium with the quinonoid intermediate II, is then protonated to yield the ALA-external aldimine (Scheme 1, *VIII*) (13). Release of ALA from the active site, guided by conformational transitions, represents the final and rate-limiting step of the catalytic cycle (11–13). Because the ALAS-catalyzed reaction is reversible (8) and the quinonoid intermediate II is also generated upon removal of the C5 proton of ALA during the reverse reaction (9, 11, 12, 14), the active site of ALAS must have evolved to minimize the non-productive transformation of ALA into the quinonoid intermediate II. However, the active site region responsible for minimizing this non-productive transformation remains unknown.

ALAS belongs to the α-oxoamine synthase (AOS) family of PLP-dependent enzymes, whose members catalyze a conden-

* This work was supported by National Institutes of Health Grant GM080270 and American Heart Association, Greater Southeast Affiliate, Grants 10GRNT4300073 and 13GRNT16970019 (to G. C. F.).
[1] To whom correspondence should be addressed: Dept. of Molecular Medicine, Morsani College of Medicine, MDC 7, University of South Florida, Tampa, FL 33612-4799. Tel.: 813-974-5797; Fax: 813-974-0504; E-mail: gferreir@health.usf.edu.
[2] The abbreviations used are: ALAS, 5-aminolevulinate synthase; ALA, 5-aminolevulinate; mALAS2, murine erythroid ALAS; PLP, pyridoxal 5′-phosphate; AOS, α-oxoamine synthase; AONS, 8-amino-7-oxononanoate synthase; SPT, serine palmitoyltransferase; PDB, Protein Data Bank; KBL, 2-amino-3-ketobutyrate-CoA ligase.

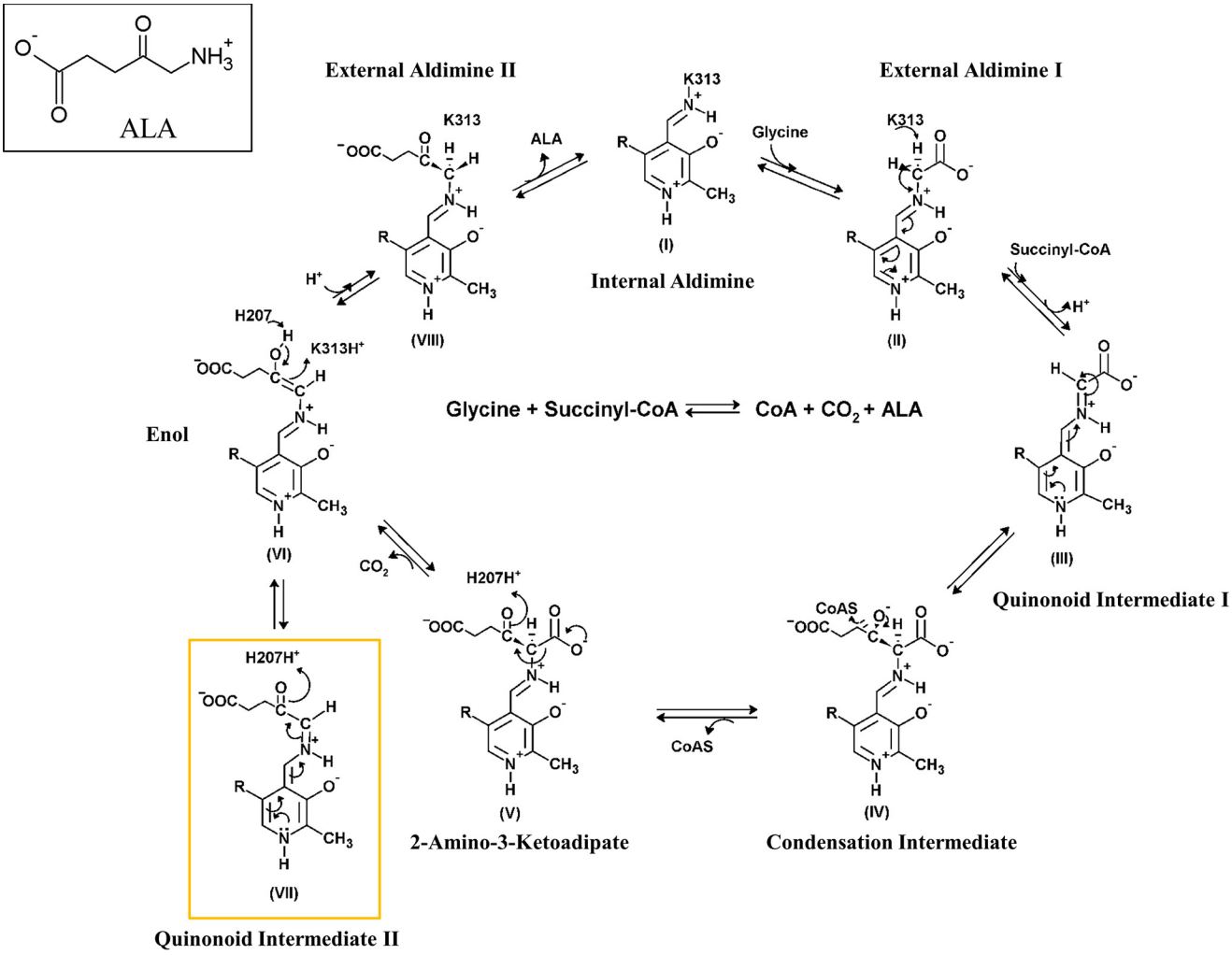

SCHEME 1. **Postulated mechanistic cycle for the mALAS2-catalyzed reaction.**

sation between an amino acid substrate and acyl-CoA (1). The AOS family also includes 8-amino-7-oxononanoate synthase (AONS) (15, 16), serine palmitoyltransferase (SPT) (17–20), and 2-amino-3-ketobutyrate-CoA ligase (KBL) (21), which, respectively, participate in biotin and sphingolipid biosynthesis, and threonine catabolism. Two other enzymes, CqsA and LqsA (22–24), involved in quorum sensing, have also been recently grouped in the AOS family. Even though ALAS shares a conserved fold and catalytic mechanism with the other AOS enzymes (except for KBL, which only catalyzes substrate condensation, without the subsequent decarboxylation of the keto acid (21)), the enzyme shows strict specificity for glycine (9, 10, 25), and thus cannot utilize the physiological amino acid substrates of AONS (L-alanine) and SPT (L-serine) (15, 17). This specificity toward glycine stems in part from the positioning of an active site threonine (Thr-83 in *Rhodobacter capsulatus* ALAS; Thr-148 in murine erythroid ALAS (abbreviated as mALAS2)) (9, 10, 25), which is located in a glycine-rich stretch from the opposite monomer (*R. capsulatus* ALAS amino acids 77′–89′). Interestingly, during the formation of the L-serine (or L-threonine)[3] external aldimine, hysteretic behavior is observed, as monitored in the kinetic trace of the wild-type ALAS reaction but not in that of the substrate-promiscuous T148A variant (9). These findings implicate that steric constraints imposed by the active site of wild-type ALAS contribute toward the amino acid substrate specificity.

Recently, we have identified an alternative channel in *R. capsulatus* ALAS that serves as a potential path for the entry of glycine into the active site and/or the exit of ALA from the active site (Fig. 1) (9). The architecture of this channel is shaped by amino acids from the C-terminal (*i.e. R. capsulatus* ALAS amino acids 337–352) and N-terminal (*i.e. R. capsulatus* ALAS amino acids 1–24) domains of one monomer and by the glycine-rich stretch from the opposite monomer (*i.e. R. capsulatus* ALAS amino acids 77′–89′) (Fig. 1), which, as discussed above, is important in defining the amino acid substrate specificity (9, 10, 25). Asn-85′ (Asn-150′ of mALAS2) of this glycine-rich stretch appears to play a particularly important role in mediating the opening and closing of this channel. Upon careful analysis of the crystal structure of *R. capsulatus* ALAS (26), we observed that, in the closed conformation, Asn-85′ is within an H-bond distance with Gln-359 of the flexible active site loop (Gln-424 of mALAS2; the distance between Asn-85′/$O^{\delta 1}$ from chain A and Gln-359/$N^{\epsilon 1}$ from chain B is 2.5 Å (Fig. 2)). Inter-

[3] B. M. Stojanovski and G. C. Ferreira, unpublished data.

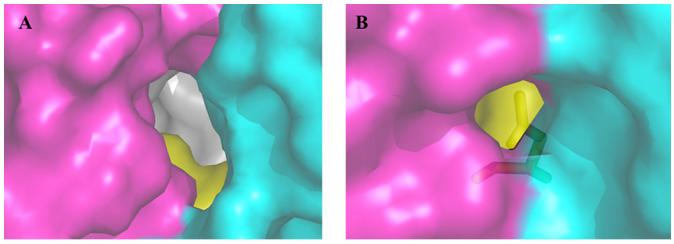

FIGURE 1. **Alternative channel leading to the active site of *R. capsulatus* ALAS in the open (*A*) and closed (*B*) conformations**. In the closed conformation, the repositioning of the side chain of Asn-85′ (*yellow sticks*) results in closure of the channel. The N-terminal domain is shown in *cyan*, the catalytic domain in *gray*, and the C-terminal domain in *magenta*, and the opposite monomer is shown in *yellow*. The image was created by aligning the A and B monomers of PDB code 2BWN with those of 2BWO using PyMOL.

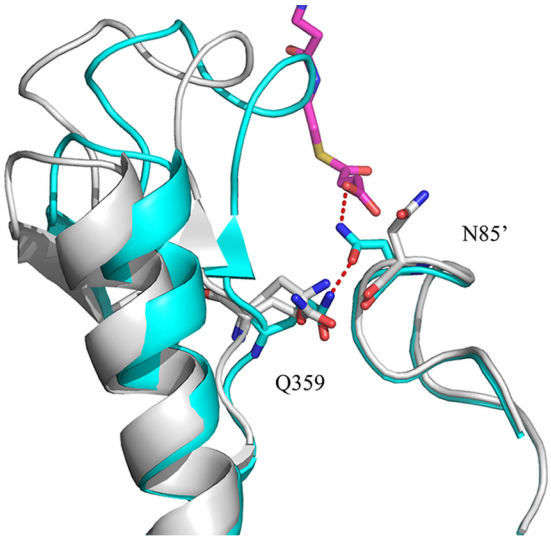

FIGURE 2. **Side chain of Asn-85′ becomes reoriented during the closed (*cyan*) to open (*gray*) conformational transition in *R. capsulatus* ALAS.** In the closed conformation (PDB code 2BWO), the distance between Asn-85′/$O^{\delta 1}$ from chain A and Gln-359/$N^{\epsilon 1}$ from chain B is 2.5 Å. In the open conformation (PDB code 2BWN), the distance increases to 5.3 Å. Asn-85′ in *R. capsulatus* ALAS corresponds to Asn-150′ in mALAS2. Succinyl-CoA is shown in *magenta*. The image was created by aligning the A and B monomers of PDB code 2BWN with those of 2BWO using PyMOL.

action between these amino acids promotes closure of the channel. In contrast, when ALAS reverts to the open conformation, this interaction is disrupted, and the side chain of Asn-85′ is reoriented away from the active site loop, which, in turn, results in opening of the channel (Fig. 2). Apart from gating the active site from the solvent, Asn-85′ also plays a vital role in positioning the carboxyl group of succinyl-CoA (Fig. 2) (10, 26). Moreover, once condensation with glycine occurs, the succinyl-derived carboxyl group of the resulting 2-amino-3-ketoadipate intermediate is expected to retain the interaction with Asn-85′, implicating an additional role of this amino acid in catalytic steps subsequent to condensation (*i.e.* in reaction steps after intermediate IV of Scheme 1).

Based on the postulated catalytic importance of this invariant asparagine, we created a small library of variants targeting Asn-150 of mALAS2 and characterized the catalytic properties of the N150H and N150F variants. These variants were selected, to a great extent, because in other AOS enzymes Asn-150 is substituted by a histidine or a phenylalanine. Our results, derived from steady- and pre-steady-state kinetic analyses, indicate that evolutionary pressure favored the selection of Asn-150 to optimize the forward reaction, at the expense of the reverse reaction, thus endowing ALAS with selectivity toward ALA production and ensuring that ALA is predominantly utilized for heme biosynthesis.

Experimental Procedures

Reagents—The following reagents were obtained from Fisher: glycine, potassium phosphate monobasic, potassium phosphate dibasic, HEPES, glycerol, and sodium hydroxide. A bicinchoninic acid assay kit was from Thermo Scientific. 5-Aminolevulinate hydrochloride was from Acros Organics, and pyridoxal 5′-phosphate, bovine serum albumin (BSA) standards, DEAE-resin, and ACA-44 ultrogel were from Sigma.

Construction of Library of Variants—Mutations at positions Thr-148 and Asn-150 were introduced simultaneously using combinatorial active site saturation test (27). The strategy used for designing the library of constructs was similar to those previously described (28, 29). Staggered oligomers with 15 complementary oligonucleotides were designed to span the wild-type mALAS2 cDNA sequence between the KpnI and AvrII restriction sites. The forward oligomer with the KpnI site contained random nucleotides at positions 148 and 150 (5′-TGC T*GG TAC C*TG AGA TVN NGC GWN NGC CCC CAG CTC CAG CTC CAT GAT TCT TCA GGG T-3′), where N = 25% A + 25% C + 25% G + 25% T; V = 33% A + 33% G + 33% C; W = 50% A + 50% T (mutated codons are underlined and the sequence for the KpnI site is in *italics*). The mutagenic oligonucleotides included the codons for all naturally occurring amino acids at position Asn-150, whereas at Thr-148 only tryptophan was excluded. Oligonucleotide B, previously described in Ref. 28, was used as the reverse oligomer. (See Ref. 28 for sequence of oligonucleotide B.) An annealing reaction, with a final volume of 6 μl and containing 60 pmol of each oligonucleotide, was incubated at 65 °C for 2 min and slowly cooled down to room temperature. The annealed oligonucleotides were extended at room temperature for 20 min in a reaction containing 2.5 units of Vent polymerase, 33 μM dNTPs mixtures, and Vent reaction buffer. This double-stranded DNA served as template for PCR amplification (temperature, duration, and number of PCR cycles as in Ref. 28), and the resulting PCR product was digested with KpnI and AvrII restriction endonucleases and subcloned into a vector previously digested with the same endonucleases.

Screening and Selection of Functional ALAS Variants—Selection of functional mALAS2 variants from the Thr-148/Asn-150 library of constructs was accomplished by reversing the ALA auxotrophic phenotype of *Escherichia coli hemA*$^-$ (HU227) cells (30) as described elsewhere (28, 29). High throughput sequencing was used to identify the introduced mutations (University of Florida, Interdisciplinary Center for Biotechnological Research).

Overproduction and Purification of Wild-type mALAS2 and Variant Enzymes—Wild-type mALAS2 and the variant enzymes were overproduced and purified as described previously (31). All purification steps subsequent to cell lysis were performed in 1 day, and the concentrated proteins were stored under liquid nitrogen for further use. All enzymes were purified

to homogeneity as assessed by SDS-PAGE. The protein concentration of the enzymes used for steady-state kinetic analyses was determined by the bicinchoninic acid-based assay using BSA as standards and measuring the absorbance of each sample and standard at 532 nm after incubation at 37 °C for 30 min as specified in the protocol supplemented by the manufacturer (Thermo Scientific). Protein concentration of enzymes used in pre-steady-state kinetic analyses was determined spectroscopically (32).

Steady-state Kinetics—Steady-state activities of the wild-type mALAS2 and variant enzymes were determined using a continuous spectrophotometric assay (33). All assays were performed in 20 mM HEPES, pH 7.5, containing 10% glycerol and at either 30 or 37 °C and monitored with a Shimadzu UV-2401 PC spectrophotometer. The pertinent final concentrations in the assays were 2 μM enzyme (wild-type mALAS2 or variant), 5–200 mM glycine, and 0.5–20 μM succinyl-CoA. The steady-state kinetic parameters (k_{cat} and K_m) were calculated by fitting the data, collected as matrices of five glycine and five succinyl-CoA concentrations, to the Michaelis-Menten equation (Equation 1) using non-linear regression analysis (SigmaPlot software).

$$V = \frac{V_{max}[S]}{K_m + [S]} \quad \text{(Eq. 1)}$$

Equilibrium Dissociation Constants for Succinyl-CoA and CoA—Equilibrium dissociation constants for succinyl-CoA or CoA were determined by titrating each of the enzymes (wild type or variants) with increasing concentrations of ligand and monitoring the quenching of intrinsic fluorescence at 340 nm upon excitation at 280 nm. The titration experiments were performed at 37 °C and pH 7.5 and monitored using a Shimadzu RF5301 PC spectrofluorophotometer. Briefly, 1 μM enzyme in 20 mM HEPES, pH 7.5, containing 10% glycerol was titrated with small aliquots of increasing concentrations of succinyl-CoA or CoA (from a 24 mM stock for wild-type and N150H and 22 mM for N150F) while stirring, until no further change in fluorescence emission was observed. The addition of ligand did not result in significant changes in the reaction volume (~4% change in the final volume), and it did not affect the pH of the buffer. The protein and ligands were equilibrated within the cell for 1 min prior to collecting the spectra. To obtain the fraction of ligand bound (F.B.) to the enzyme, data were normalized using Equation 2,

$$\text{F.B.} = \frac{x - x_i}{x_f - x_i} \quad \text{(Eq. 2)}$$

where x represents the maximal fluorescence emission at a specific ligand concentration; x_i is the emission in the absence of ligands; and x_f is the emission at the highest concentration of ligand when the enzyme was fully saturated. The equilibrium dissociation constant, K_d, was determined by fitting the data to Equation 3, using SigmaPlot software for the non-linear regression analyses.

$$Y = \frac{Y_{max}[S]}{K_d + [S]} \quad \text{(Eq. 3)}$$

Pre-steady-state Kinetics—Reactions between the enzyme (mALAS2 or variant)-glycine complex and succinyl-CoA were analyzed using transient kinetics. Upon rapid mixing of the enzyme-glycine complex with succinyl-CoA, single-wavelength spectra were collected at 510 nm on a KinTek stopped-flow spectrophotometer (model SF-2001). Prior to the kinetic measurements, the purified concentrated proteins were dialyzed into a 50 mM phosphate, pH 7.5, buffer with 10% glycerol (v/v) and 40 μM PLP. All reactions were performed at 18 °C using a buffer composed of 50 mM phosphate, pH 7.5 (37 mM K_2HPO_4, 13 mM KH_2PO_4), and 10% glycerol (v/v). For reactions under single turnover conditions, with the enzyme molar concentration in excess over that of succinyl-CoA, one of the syringes contained 120 μM enzyme (either wild-type mALAS2 or variant) and 200 mM glycine in the above described buffer, whereas the other syringe contained 40 μM succinyl-CoA in the same buffer. The concentrations of reactants in the observation cell were one-half of those in the syringes. For reactions conducted under multiple turnover conditions, with succinyl-CoA in excess over enzyme, one of the syringes contained 60 μM enzyme (either wild-type mALAS2 or variant) and 200 mM glycine in the above phosphate buffer, whereas the other syringe contained excess succinyl-CoA in the same buffer. Using the KinTek stopped-flow software, the time course data were fitted to either a two- or three-exponential equation (Equation 4),

$$A_t = \sum_{n=1}^{3} a_i e^{-k_i t} + c \quad \text{(Eq. 4)}$$

where A_t is the absorbance at time t; a is the amplitude of each phase; k is the observed rate constant for each phase, and c is the final absorbance. The reaction between wild-type mALAS2 or variant enzymes and ALA was also examined using transients by monitoring the change in absorbance at 510 nm upon rapid mixing of the reactants. One of the syringes contained 60 μM enzyme in the above 50 mM phosphate buffer, and the other syringe contained ALA in the same buffer. Prior to reacting mALAS2 (or the variants) with ALA, the ALA-HCl stock was neutralized in equal molar concentration of NaOH. This was accomplished by creating 2-fold serial dilutions of ALA and NaOH, where the final concentration of ALA in the observation chamber, neutralized in equal molar concentration of NaOH, varied from 0.5 to 30 mM. Once the reaction was completed, it was verified that the pH in the syringe was 7.5. The dependence of the observed first order rate constants on the concentration of ALA was fitted to an equation describing a two-step reaction (Equation 5), using non-linear regression analyses (SigmaPlot software).

$$k_{obs} = \frac{k_2[S]}{K_d[S]} + k_{-2} \quad \text{(Eq. 5)}$$

Results

Asn-150 Library of Constructs and Screening of Functional mALAS2 Variants—Combinatorial active site saturation test (27) was used to introduce mutations at positions Thr-148 and Asn-150 of the glycine-rich stretch of mALAS2. The combinatorial active site saturation test combines the features of ratio-

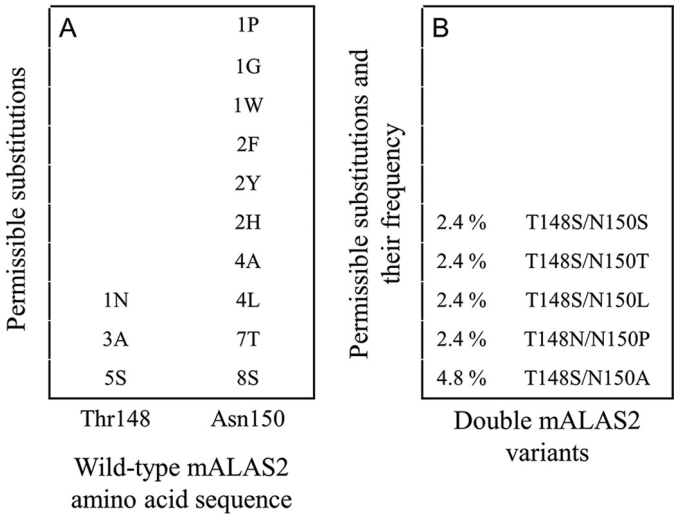

FIGURE 3. **Permissible amino acid substitutions identified at positions Thr-148 and Asn-150 of mALAS2.** *A,* frequency of the substitutions at amino acid positions 148 and 150 of mALAS2. The *number* in front of the one-letter amino acid code indicates the total number of functional substitutions at that position identified in the library of constructs. *B,* frequency of simultaneous substitutions at amino acid positions 148 and 150 of mALAS2. The *percentage* (%) in front of the one-letter amino acid code for the two mutations indicates the percentage of functional substitutions at those positions identified in the library of constructs.

nal design and combinatorial amino acid randomization at specific sites, allowing for the design of small libraries of variant enzymes produced by randomization at sets of two spatially close amino acids in the active site (27). We screened for functional variants by transforming and reversing the ALA auxotrophic *E. coli* HU227 cells phenotype (30). Approximately 10% of the over 500 screened colonies grew in the absence of ALA, indicating that the growth of *E. coli* HU227 cells had been rescued due to the harbored recombinant, putative mALAS2 variant(s). Plasmid DNA isolated from 52 of these colonies was sequenced to verify the nature of the introduced mutations. Around 90% of the functional constructs contained mutations at positions 148 and 150, which are occupied by Thr and Asn in wild-type mALAS2, whereas the other 10% corresponded to the wild-type mALAS2 amino acids. It should be noted that, with the design of the mutagenic primers, the introduction of codons for the wild-type amino acids at positions 148 and 150 could not be prevented. The complete list of permissive substitutions is shown in Fig. 3. Seven independent and singly introduced amino acids (Ser, Thr, Phe, His, Ala, Gly, and Trp) were tolerated at position 150 occupied by Asn in wild-type mALAS2, although the frequency of introduced mutations varied. Among the functional variants, mutation of Asn-150 to Ser occurred 10 times more frequently than to either Gly or Trp and 5 times more frequently than to either His or Phe. However, substitution of Asn-150 with Pro only emerges when accompanied by mutation of Thr-148. In contrast, Thr-148 only accepted Ala as a single permissive substitution, and all other amino acid replacements needed to be concomitant with substitution of Asn-150 to produce functional mALAS2 variants (Fig. 3).

Initial Kinetic Studies and Rationale for Selection of Functional N150H and N150F Variants for Further Detailed Characterization—The steady-state kinetic parameters and specificity constants of five of the seven isolated functional variants with only Asn-150 mutations were determined at pH 7.5 and 30 °C (Table 1). This temperature was chosen for initial characterization of the steady-state kinetic properties because the majority of our studies on wild-type mALAS2 and mALAS2 variants involving enzymatic activity determinations have been conducted at 30 °C (29, 34, 35). Relative to the wild-type enzyme, the most pronounced reduction in the k_{cat} value was observed with the N150H and N150F variants, although the N150W mutation also reduced the turnover rate by about 40% (Table 1). The N150A and N150S mutations did not significantly perturb the steady-state kinetic parameters of mALAS2 (Table 1).

The purification yields of the N150W variant were typically poor, which made it technically difficult for us to pursue with the characterization of this enzyme, particularly the pre-steady-state kinetic studies, which require considerably high concentrations of purified protein. In addition, the purification of the double variant, T148S/N150P, to homogeneity remained unattainable, and we had to relinquish its potential examination. Our selection of the N150H and N150F variants as a means to investigate the role of Asn-150 in mALAS2 catalysis was based on two criteria: 1) the N150H and N150F mutations had the greatest effect on the steady-state kinetic parameters of mALAS2, and 2) histidine and phenylalanine occupy the analogous position to Asn-150 in the glycine-rich stretch of other AOS enzymes. Specifically, superimposition of the crystal structure of *R. capsulatus* ALAS (PDB 2BWO) with those of AONS, KBL, and SPT (data not shown) revealed that Asn-85 (Asn-150 of mALAS2) is substituted by a histidine in *E. coli* AONS (His-78 in PDB 1DJE) (16), and by a phenylalanine in *E. coli* KBL (21) and *Sphingobacterium multivorum* SPT (Phe-81 in PDB 1FC4 and Phe-83 in PDB 3A2B) (18). Phenylalanine is also present in *Vibrio cholerae* CqsA (Phe-79 in PDB 3KKI (23)) but, unlike in other AOS enzymes, Phe-79 makes a short helical element that is part of an extended loop (22, 23), with no glycines (data not shown). This extended loop is disordered in the apoenzyme structure of CqsA but not in the substrate-bound enzymes (22). Interestingly, the crystal structure of *Sphingomonas paucimobilis* SPT indicates that methionine (Met-104 in PDB 2JG2) (19) takes the place of the asparagine found in the ALAS glycine-rich stretch. However, there were no functional variants with methionine substitutions at position 150 in our library of constructs (Fig. 3). Finally, because we and others previously reported findings on the catalytic role of Thr-148 in mALAS2 (Thr-83 in *R. capsulatus* and *Rhodobacter sphaeroides* ALAS) (9, 10, 25), the focus of this study is on the role of Asn-150.

Steady-state Kinetics and Specificity Constants of the N150H and N150F Variants—The steady-state kinetic parameters and specificity constants for wild-type mALAS2, N150H, and N150F were also determined at 37 °C and pH 7.5 (Table 2). The N150H and N150F mutations resulted in respective decreases of 64 and 56% in the k_{cat} values, with no significant changes in K_m^{SCoA}. A 4-fold increase in the K_m^{Gly} was noted for the N150H variant. Interestingly, the k_{cat} reported here for mALAS2, which does not have a N-terminal His tag, is 2.6-fold lower than the one reported by Tan *et al.* (36) at identical temperature for the N-terminal His-tagged wild-type enzyme. However, in that

TABLE 1
Steady-state kinetic parameters and specificity constants determined at 30 °C and pH 7.5

Enzyme	k_{cat}	K_m^{Gly}	K_m^{SCoA}	k_{cat}/K_m^{Gly}	k_{cat}/K_m^{SCoA}
	s^{-1}	m_M	μ_M	$s^{-1}\cdot m_M^{-1}$	$s^{-1}\cdot \mu_M^{-1}$
WT mALAS2[a]	0.16 ± 0.02	23 ± 1	2.3 ± 0.1	$7 \times 10^{-3} \pm 1 \times 10^{-3}$	$70 \times 10^{-3} \pm 11 \times 10^{-3}$
N150A	0.13 ± 0.007	16 ± 4	3.8 ± 0.7	$8.1 \times 10^{-3} \pm 2 \times 10^{-3}$	$34 \times 10^{-3} \pm 8 \times 10^{-3}$
N150S	0.15 ± 0.01	11 ± 1.6	2.1 ± 0.4	$13.6 \times 10^{-3} \pm 2.8 \times 10^{-3}$	$71 \times 10^{-3} \pm 18 \times 10^{-3}$
N150W	0.09 ± 0.01	39 ± 14	1.1 ± 0.6	$2.3 \times 10^{-3} \pm 1 \times 10^{-3}$	$82 \times 10^{-3} \pm 50 \times 10^{-3}$
N150H	0.04 ± 0.002	16 ± 5	1.2 ± 0.2	$2.5 \times 10^{-3} \pm 0.9 \times 10^{-3}$	$33 \times 10^{-3} \pm 7 \times 10^{-3}$
N150F	0.06 ± 0.001	12 ± 0.7	2.2 ± 0.1	$5 \times 10^{-3} \pm 0.4 \times 10^{-3}$	$27 \times 10^{-3} \pm 1.6 \times 10^{-3}$

[a] Kinetic constants for WT mALAS2 were reported in Ref. 34.

TABLE 2
Steady-state kinetic parameters and specificity constants determined at 37 °C and pH 7.5

Enzyme	k_{cat}	K_m^{Gly}	K_m^{SCoA}	k_{cat}/K_m^{Gly}	k_{cat}/K_m^{SCoA}
	s^{-1}	m_M	μ_M	$s^{-1}\cdot m_M^{-1}$	$s^{-1}\cdot \mu_M^{-1}$
WT mALAS2	0.25 ± 0.004	8 ± 0.7	1.0 ± 0.1	$31 \times 10^{-3} \pm 3 \times 10^{-3}$	$250 \times 10^{-3} \pm 29 \times 10^{-3}$
N150H	0.09 ± 0.002	32 ± 4	1.2 ± 0.2	$2.8 \times 10^{-3} \pm 0.4 \times 10^{-3}$	$75 \times 10^{-3} \pm 14 \times 10^{-3}$
N150F	0.11 ± 0.002	13 ± 2	2.3 ± 0.3	$8.5 \times 10^{-3} \pm 1 \times 10^{-3}$	$47 \times 10^{-3} \pm 7 \times 10^{-3}$

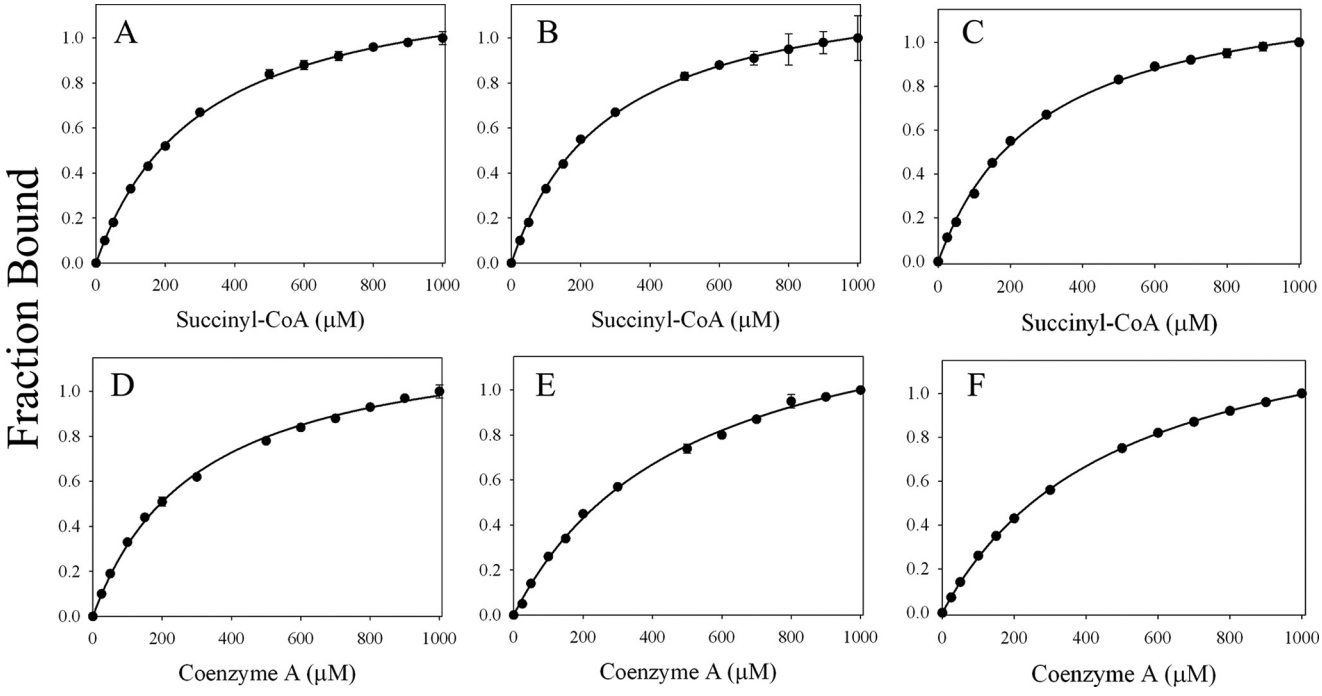

FIGURE 4. **Binding isotherms for the association of succinyl-CoA or CoA with wild-type mALAS2, N150H, or N150F.** Titration of wild-type mALAS2 (*A*), N150H (*B*), and N150F (*C*) with increasing concentrations of succinyl-CoA and titration of wild-type mALAS2 (*D*), N150H (*E*), and N150F (*F*) with increasing concentrations of CoA.

study, the enzyme concentration was estimated using a BCA-based assay after the protein was precipitated with acetone (4, 36). We validated that acetone precipitation can lead to underestimation of the protein concentration (data not shown), and thus, the disparities in the reported k_{cat} values largely result from differences in the methods used to quantify the protein concentration and not from the presence of a His tag.

Equilibrium Dissociation Constants for Succinyl-CoA and CoA—The equilibrium dissociation constant (K_d) values for succinyl-CoA and CoA were determined at 37 °C and at pH 7.5 by monitoring the quenching in intrinsic protein fluorescence upon titration of the wild-type or variant enzymes (N150H and N150F) with increasing concentrations of ligand (Fig. 4). Wild-type mALAS2 exhibited equal binding affinity toward succinyl-CoA and CoA, implying that binding is primarily facilitated by the CoA moiety (Table 3). Moreover, the wild-type, N150H, and N150F enzymes have identical K_d^{SCoA} values, within error, whereas both variants displayed weaker binding toward CoA (Table 3). Because CoA lacks a succinyl moiety, the results suggest an important role for the succinyl moiety in the binding of succinyl-CoA to the active site of the N150H and N150F variants. Importantly, for the wild-type and variant enzymes, there are significant differences between the K_m and K_d values for succinyl-CoA(Tables 2 and 3 and see "Discussion").

Single Turnover Experiments—Pre-steady-state reactions between the enzyme (wild-type or variant)-glycine complex and succinyl-CoA were conducted under single turnover conditions, with enzyme concentrations in excess over those of succinyl-CoA, and followed by monitoring the changes in absorbance at 510 nm that result from the formation of the quino-

TABLE 3
Equilibrium dissociation constants for succinyl-CoA and CoA

Enzyme	K_d^{SCoA}	K_d^{CoA}
	μM	μM
WT mALAS2	297 ± 7	302 ± 12
N150H	281 ± 7	495 ± 25
N150F	284 ± 10	486 ± 6

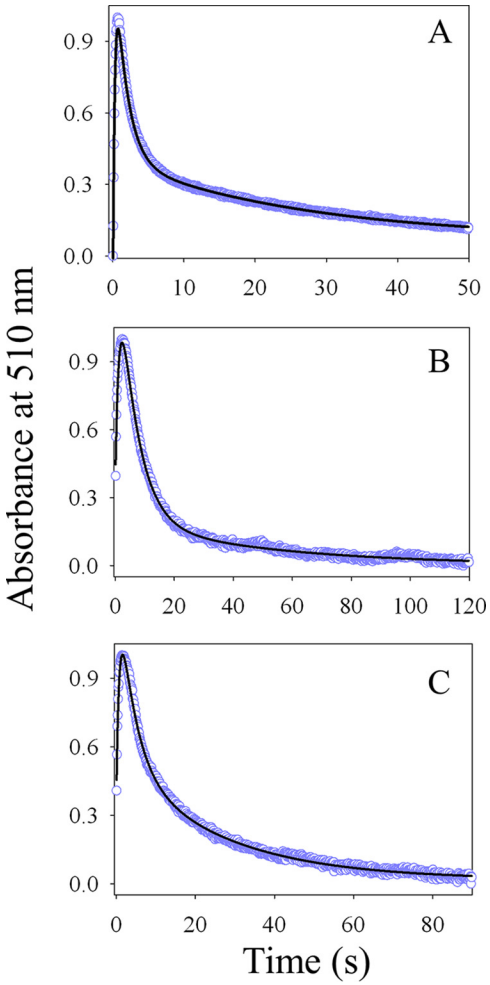

FIGURE 5. **Kinetic traces of the reactions of the enzyme (wild-type or variant)-glycine complex with succinyl-CoA under single turnover conditions.** The kinetic traces for the reactions of wild-type mALAS2-glycine (*A*), N150H-glycine (*B*), and N150F-glycine (*C*) complexes with 20 μM succinyl-CoA (*purple circles*), as followed by monitoring the changes in the quinonoid intermediate absorbance at 510 nm, were overlaid with the lines (*black*) calculated from the data fitting to Equation 4 for a three-exponential process. The reported succinyl-CoA concentration is that in the observation chamber.

noid intermediate II (Fig. 5 and Scheme 1, *VII*). Also as in previous studies (13, 29), we used excess glycine (over 7-fold the dissociation constant (34)) to ensure that the enzyme (mALAS2 or variant) was trapped in the glycine-bound form, and the second step of the quinonoid intermediate II decay approached the rate of ALA release from the enzyme. This way, the ALA produced during the single turnover is not expected to compete with glycine for binding to the enzyme, as ALA binds tightly and forms a quinonoid intermediate (A_{max} = 510 nm), and glycine does not bind tightly and is predominantly converted into an external aldimine (A_{max} = 420 nm) (13). Because of the rapid formation and transient nature of the quinonoid intermediate II, it was challenging to accurately discern the individual kinetic phases at 37 °C, and consequently, the reaction was monitored at 18 °C and pH 7.5. The reactions for either the wild-type or variant enzymes are best described by a three-exponential process (Fig. 5). Previous extensive single turnover experiments with mALAS2 have led to the assignment of the following three kinetic steps: 1) generation of the quinonoid intermediate II (Scheme 1, *VII*) upon decarboxylation of the 2-amino-3-ketoadipate intermediate (Scheme 1, *V*); 2) decay of this quinonoid intermediate, as facilitated by protonation of the enol (Scheme 1, *VI*) by Lys-313; and 3) conformational rearrangement of the enzyme to induce ALA release from the active site (Scheme 1, dissociation of *VIII*) (13). Significantly, the rate constant (k_3) value calculated from the single turnover experiments (13, 29, 35) approximates the off-rate constant (k_{-1}), ascribed to a protein conformational transition step associated with product release, as determined by monitoring the quenching of intrinsic protein fluorescence upon binding of ALA to wild-type mALAS2 (35). Although this assignment is likely equally valid for the experiments reported here, the possibility that the third observed kinetic step is associated with steady-state level of quinonoid intermediate II cannot be ruled out. Presented in Table 4 are the three observed rate constants for the reactions catalyzed by the wild-type and variant enzymes. Significant decreases in the rates of formation of the quinonoid intermediate II were detected for the N150H- and N150F-catalyzed reactions, with the values of $k_1 = 0.81 \pm 0.02\ s^{-1}$ and $k_1 = 1.36 \pm 0.03\ s^{-1}$ for the respective observed rate constants (Table 4). These rate constants for the reactions of the N150H and N150F variants are by 79 and 64% lower than that of the wild-type enzyme, respectively. Furthermore, the mutations resulted in reductions in the rates of quinonoid intermediate II decay (Table 4). The data implicate an important role for Asn-150 in catalysis, probably by stabilizing the positioning of the condensation intermediate in an orientation that is energetically favorable for its conversion into the quinonoid intermediate II.

TABLE 4
Observed rate constants for the reaction between the enzyme-glycine complex and succinyl-CoA

Enzyme	k_1[a]	k_2[b]	k_3[c]
	s^{-1}	s^{-1}	s^{-1}
WT mALAS2	3.8 ± 0.03	0.59 ± 0.005	0.038 ± 0.001
N150H	0.81 ± 0.02	0.16 ± 0.002	0.020 ± 0.001
N150F	1.36 ± 0.03	0.25 ± 0.01	0.039 ± 0.001

[a] Rate for quinonoid intermediate II formation.
[b] Rate for first step of quinonoid intermediate II decay.
[c] Rate for second step of quinonoid intermediate II decay.

Multiple Turnover Experiments—The transient reaction between the enzyme-glycine complex and succinyl-CoA, monitored by following the absorbance changes at 510 nm, was also conducted under multiple turnover conditions (18 °C and pH 7.5), with succinyl-CoA concentration in excess over those of the enzyme. Although the reactions catalyzed by the wild-type enzyme were best described by a biphasic process, corresponding to the formation of the quinonoid intermediate II followed by its steep decay into the steady state (Fig. 6, *A–C*), the progress curves of the N150H variant-catalyzed reactions displayed an apparent prolonged decay of the quinonoid interme-

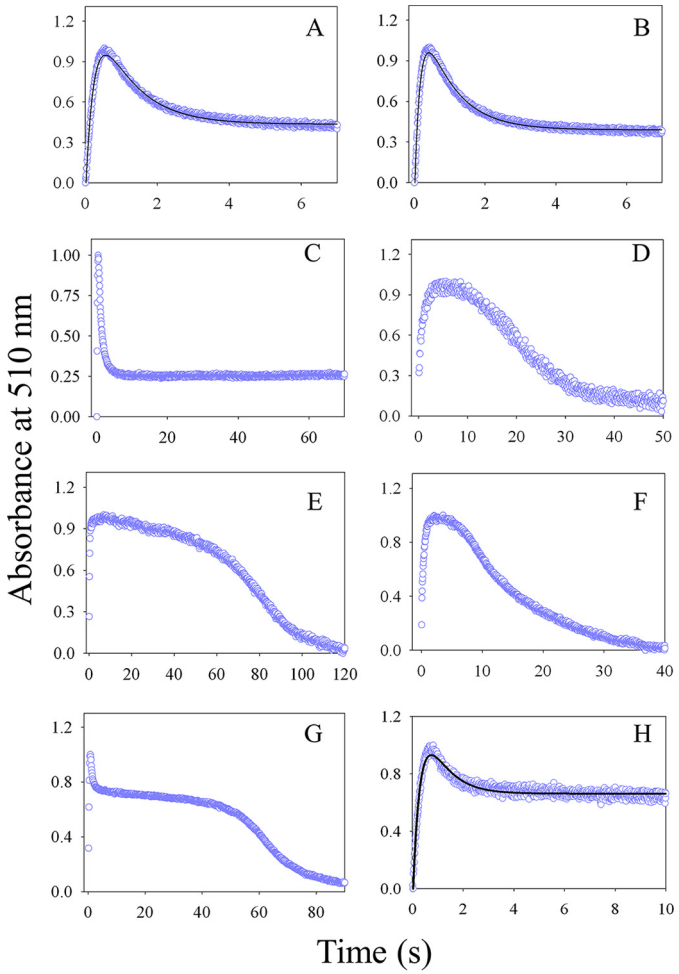

FIGURE 6. **Kinetic traces of the reactions of the enzyme (wild-type or variant)-glycine complex with succinyl-CoA under multiple turnover conditions.** Progress curves, as monitored from the changes in absorbance at 510 nm, were collected for the reactions between the wild-type mALAS2-glycine complex (30 μM) and 30 μM (*A*) and 160 μM (*B*) succinyl-CoA. *C*, 70-s time course for the wild-type reaction with 160 μM succinyl-CoA is shown. Progress curves were collected for the N150H-glycine complex (30 μM) reacted with 30 μM (*D*) and 160 μM (*E*) of succinyl-CoA and for the N150F-glycine complex (30 μM) reacted with 30 μM (*F*) and 160 μM (*G*) of succinyl-CoA. *H*, initial 10-s time course for the N150F reaction with 160 μM succinyl-CoA is shown. Where applicable (*A, B,* and *H*), the data were fitted to a two-step exponential equation, and the data points (*purple*) are overlaid with the fitted line (*black*).

diate II into the steady state (Fig. 6, *D* and *E*). This precluded us from fitting the data for the N150H-catalyzed reactions to a two-exponential equation, without significant residual error (data not shown). The extent of this prolonged decay was less pronounced for the N150F reaction (Fig. 6, *F–H*), although the kinetic trace was clearly different from that of the reaction for the wild-type enzyme. Lowering the succinyl-CoA concentration in the N150H- and N150F-catalyzed reactions resulted in a more rapid decay of the quinonoid intermediate II, implying potential accumulation of reaction intermediates absorbing at the wavelength of interest (Fig. 5). Of note, in some reactions (see Fig. 5 legend), we violated the multiturnover premise by lowering the succinyl-CoA concentration to 30 μM with the aim of showing that the decay of the kinetic trace displayed dependence on the concentration of succinyl-CoA.

Reaction of ALA with Either Wild-type or Variant Enzymes—Because the kinetic trace for the multi-turnover reaction for the variant reactions revealed a prolonged decay of the quinonoid intermediate II into the steady state (Fig. 6), which may have resulted from accumulation and transformation of ALA back into the quinonoid intermediate II (Scheme 1), we set to examine the mALAS2-, N150H-, and N150F-catalyzed reverse reactions with ALA (pH 7.5 and 18 °C) using stopped-flow spectroscopy. Previously, we demonstrated that binding of ALA to ALAS is followed by the formation of a stable quinonoid intermediate (Scheme 1, *VII*) with a characteristic absorbance maximum at 510 nm (11, 12). A biphasic process describes the time courses for the reactions of wild-type mALAS2, N150H, or N150F with ALA, when monitored at 510 nm (Fig. 7). In agreement with previous studies (11, 12), the observed rates for the second and slow phase of the wild-type mALAS2 reaction were independent of the ALA concentration, while the observed rates associated with the fast phase rate displayed hyperbolic dependence on the ALA concentration (Fig. 7). The rate constants (k_2 and k_{-2}) and dissociation constant (K_d) associated with the fast phase were obtained by fitting the data for the ALA-dependent observed rates (Fig. 7, *B–D*) to Equation 5. The minimal mechanism used to describe the fast phase is presented in Scheme 2. The yielded values for the fast phase (*i.e.*, k_2, k_{-2}, and K_d) along with the rate constant for the slow phase (k_{slow}) for the wild-type- and variant enzyme-catalyzed reactions are reported in Table 5. As with wild-type mALAS2, the reaction between ALA and either N150H or N150F occurs in three kinetic steps. The fast phase of the wild-type mALAS2-catalyzed reaction is characterized by a rapid equilibrium with a $K_d = 2.5 \pm 0.2$ mM and rate constants $k_2 = 0.61 \pm 0.01$ s^{-1} and $k_{-2} = 0.16 \pm 0.01$ s^{-1}. We assign the fast phase of the reaction to rapid binding of ALA to the enzyme followed by the chemical conversion of ALA into the quinonoid intermediate II (Scheme 1, *VII*, and Scheme 2). The slow phase, whose observed rate is independent of ALA concentration, probably represents a conformational transition of the enzyme. Interestingly, it was previously reported that the rate constant for the slow phase (k_{slow}) of ALA-quinonoid intermediate formation approximates the k_{cat} when both rate constants are determined at 30 °C ($k_{slow} = 0.15$ s^{-1} (11); $k_{cat} = 0.16$ s^{-1} (34)). Similarly, in this study, the rate of the slow phase of the wild-type reaction with ALA ($k_{slow} = 0.046$ s^{-1}), which we measured at 18 °C, also approximates the reported k_{cat} value obtained at 20 °C ($k_{cat} = 0.02$ s^{-1}; value from Ref. 29).

Similar to the wild-type mALAS2-catalyzed reaction, the observed rates for the fast phase of the N150H or N150F reactions reached plateau with increasing ALA concentrations, whereas the observed slow phase rate for either reaction was ALA concentration-independent (Fig. 7). Importantly, k_2 of 1.39 ± 0.07 s^{-1} and k_2 of 1.12 ± 0.06 s^{-1} were, respectively, obtained for the fast phase rate constant of the N150H- and N150F-catalyzed formation of the ALA-quinonoid intermediate, indicating increases of 57 and 45% in the reaction rate constants relative to that of the wild-type enzyme (Table 5). Moreover, fitting the data for the fast phase rates to Equation 5 yielded K_d^{ALA} 2.5 ± 0.2 mM, K_d^{ALA} 4.7 ± 1.3 mM, and K_d^{ALA} = 2.7 ± 0.7 mM for wild-type mALAS2, N150H, and N150F,

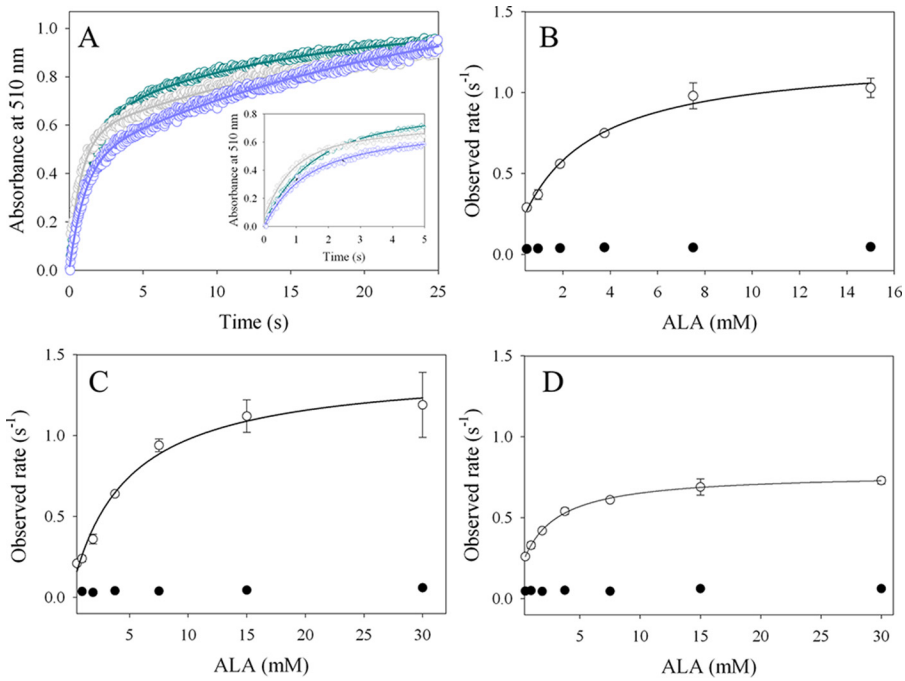

FIGURE 7. **Reactions of wild-type and variant enzymes with ALA.** *A,* progress curves for the reactions of 15 mM ALA with 30 μM of either wild-type mALAS2 (*dark cyan*), N150H (*gray*) or N150F (*purple*) were collected by monitoring the changes in absorbance at 510 nm. The initial 5 s of the kinetic traces are displayed in the *inset*. The data were fitted to a two-exponential equation, and the *fitted lines* are shown below the *circles*. *B, C,* and *D* show the ALA concentration dependences of the rates of the two phases for the N150F, N150H, and wild-type mALAS2 reactions, respectively. The ALA-dependent observed rates for the fast phase (*clear circles*) of the wild-type or variant reactions were fitted to Equation 5, and the rate constants and K_d^{ALA} values are reported in Table 5. For the wild-type or variant enzyme-catalyzed reactions, the observed rates of the slow phase (*filled circles*) were independent of the ALA concentration. All reactions were done in triplicates, and the *error bars* are shown *below* the symbols.

$$E + ALA \underset{}{\overset{K_d}{\rightleftharpoons}} E\text{-}ALA \underset{k_{-2}}{\overset{k_2}{\rightleftharpoons}} EQ_2$$

SCHEME 2. **Minimal mechanism describing the fast kinetic phase for the reaction between ALAS and ALA monitored at 510 nm.**

TABLE 5

Rate constants for the reactions of wild-type and variant enzymes with ALA

Enzyme	Fast phase			Slow phase
	K_d^{ALA}	k_2	k_{-2}	k_{slow}
	mM	s^{-1}	s^{-1}	s^{-1}
WT mALAS2	2.5 ± 0.2	0.61 ± 0.01	0.16 ± 0.01	0.046 ± 0.006
N150H	4.7 ± 1.3	1.39 ± 0.07	0.03 ± 0.07	0.039 ± 0.007
N150F	2.7 ± 0.7	1.12 ± 0.01	0.1 ± 0.06	0.043 ± 0.006

respectively (Fig. 7 and Table 5). These values are comparable, within error, with only a slight increase in the K_d^{ALA} for N150H relative to that for the wild-type enzyme.

Discussion

Because even subtle disturbances in the rate of ALA synthesis, due to loss-of-function or gain-of-function mutations in the *ALAS2* gene, result in erythropoietic disorders (such as XLSA and XLPP (5–7)), the necessity to evolve away from hypoactivity and hyperactivity must have been a defining evolutionary pressure in shaping the active site of ALAS2. Besides the critical need to synthesize ALA at a physiologically relevant rate, it can be argued that equally important evolutionary necessities, albeit quite overlooked, were for ALAS to minimize the nonproductive transformation of ALA and establish a catalytic balance between the forward and reverse reactions. The combination of these factors has probably made it possible for differentiating erythroid cells to utilize ALA predominantly for heme biosynthesis, rather than for glycine and succinyl-CoA production. However, regions of the active site contributing to the achievement of this catalytic balance have never been identified prior to this study.

Structural analysis of *R. capsulatus* ALAS revealed essential roles for Asn-85′ (Asn-150′ of mALAS2) in gating the alternative active site channel and coordinating the positioning of both succinyl-CoA (10, 26) and the condensation intermediate (Figs. 1 and 2). Based on these observations, we created a small library of constructs harboring substitutions at the position occupied by Asn-150, and we conducted detailed equilibrium and kinetic studies with the N150H and N150F variants. Our selection of these functional variants was mostly based on the finding that Asn-150 is substituted by a histidine or phenylalanine in other AOS enzymes.

Comparison of the steady-state kinetic parameters for the N150H and N150F variants with those for the wild-type enzyme indicated that the mutations resulted in decreases in the k_{cat} values by approximately one-half (Table 2). Because release of ALA from the enzyme represents the slowest step in the reaction (11, 12), our findings indicate that the amino acid substitutions introduced in the glycine-rich stretch perturb the release of product. Even though Asn-150 coordinates the positioning of succinyl-CoA, no changes in the K_m^{SCoA} value were detected with the N150H and N150F mutations. Moreover, the binding affinity toward succinyl-CoA was not perturbed by these mutations, because the K_d^{SCoA} values of the variants were identical with that of wild-type mALAS2 (Table 3). Signifi-

cantly, the determined K_d^{SCoA} value for wild-type mALAS2 (297 ± 7 μM) is comparable with the concentration of succinyl-CoA required to achieve half-maximal protection against reduction with sodium cyanoborohydride (261 ± 75 μM) (37). However, the binding of CoA to either variant was weaker than to wild-type mALAS2, although in the absence of structural information, it is difficult to rationalize how the N150H and N150F mutations weaken the affinity, particularly since Asn-150 interacts with the succinyl rather than the CoA moiety. It is possible that the substitutions indirectly perturb the integrity of the CoA-binding site. Because the crystal structure of *R. capsulatus* ALAS reveals that Asn-85′ interacts with Gln-359 of the active site loop (Fig. 2), and this loop, when it adopts the closed (but not the open) conformation, directly interacts with the pantetheine moiety of CoA, through hydrogen bonds between pantetheine N^1 and N^2 and the respective main chain carbonyl groups of the loop Thr-365 and Pro-364 (*R. capsulatus* ALAS numbering), it is plausible that the Asn-150 mutations affect the interactions with the CoA group by compromising the ability of the variants to reposition the loop in the closed conformation. These detrimental effects on the interactions with CoA might then be overcome by the binding of the succinyl moiety, which directly interacts and stabilizes the active site loop in the closed conformation (hydrogen bonds with the side chain of Thr-365), allowing for the CoA moiety to reestablish the hydrogen bonds with the carbonyl groups of the main chains of Thr-365 and Pro-364. These differences in interactions might explain why the affinity of the Asn-150 variants is weakened for CoA but not for succinyl-CoA. However, the molecular details associated with these interpretations will need to be verified experimentally, by resolving the crystal structures of the variants. Interestingly, the binding of succinyl-CoA to the wild-type enzyme is primarily facilitated by the CoA, not the succinyl, moiety, as evident from the identical K_d values for succinyl-CoA and CoA (Table 3). This finding is not unexpected because structural data (26) indicate that it is the CoA moiety of succinyl-CoA that participates in most interactions with ALAS.

Our study further revealed that the equilibrium dissociation constant, K_d^{SCoA}, which reflects the binding affinity of the enzyme toward succinyl-CoA, differs significantly from the Michaelis constant K_m^{SCoA}, which is a constant that describes the ligand concentration at which V equals ½ V_{max}. The Michaelis constant is often misinterpreted for the dissociation constant, although the two constants may or may not be equal to each other (38). In the case of wild-type ALAS, the K_d^{SCoA} value is about 300-fold greater than the K_m^{SCoA} (Tables 2 and 3). These data indicate that K_m^{SCoA} does not represent a measure of substrate affinity analogous to the k_{-1}/k_1 term, which describes the K_d, but rather it represents a complex kinetic function of multiple rate constants in the pathway. The complexity of the K_m expression of a reaction pathway containing a single intermediate, which is far less complicated than the multi-intermediate pathway of the ALAS mechanism, has been reported elsewhere (38).

The significant reductions in the observed pre-steady-state rates for the formation (k_1) and decay (k_2) of the quinonoid intermediate II (Scheme 1, *VII*) that ensued when Asn-150 was substituted with a histidine or phenylalanine strongly implicate an essential role for this asparagine in catalysis. In comparison to the wild-type enzyme, the N150H- and N150F-catalyzed reactions between glycine and succinyl-CoA, examined during a single turnover, resulted in reductions by 79 and 64% in the rate of formation of the quinonoid intermediate II, while the initial rate of quinonoid decay was reduced by 73 and 57%, respectively (Table 4). Because Asn-150 is predicted to interact with the succinyl-derived carboxyl group of the condensation intermediate (the 2-amino-3-ketoadipate intermediate (Scheme 1, *V*), which is a precursor of the quinonoid intermediate II (Scheme 1, *VII*)), it is plausible that the mutations affect the attainment of a catalytically optimal orientation between this intermediate and reactive centers. Consequently, the energetic barrier associated with its transformation into the quinonoid intermediate II is increased. Moreover, modifications in the active site environment introduced by the N150H and N150F mutations endowed the variant enzymes with a catalytic ability to transform ALA back into the quinonoid intermediate II at an accelerated rate (57 and 45% increases in the k_2 values of N150H and N150F over that of the wild-type enzyme (Table 5)).

Significantly, our results demonstrate that Asn-150 is essential for establishing a catalytic balance between the forward and reverse reactions of mALAS2 by favoring formation of ALA over its non-productive transformation into the quinonoid intermediate. We arrived at this conclusion based on the differences detected in the rates of quinonoid intermediate formation during the forward (*i.e.* with glycine and succinyl-CoA) and reverse (*i.e.* with ALA) reactions when catalyzed by the variant and wild-type enzymes (Tables 4 and 5). In fact, relative to the rate of quinonoid intermediate II formation in the forward reaction (k_1 = 3.8 ± 0.03 s^{-1}; Table 4), the wild-type enzyme transforms ALA into the quinonoid intermediate at a rate that is 6.3-fold *slower* (k_2 = 0.61 ± 0.01s^{-1}; Table 5). In contrast, the magnitudes of the rates for the N150H- and N150F-catalyzed forward and reverse reactions are strikingly different. This difference is particularly accentuated in the N150H-catalyzed reaction, with the quinonoid intermediate II formation from ALA (reverse reaction, k_2 = 1.39 ± 0.07 s^{-1}; Table 5) occurring at a rate 1.7-fold *faster* than that from glycine and succinyl-CoA (forward reaction, k_1 = 0.81 ± 0.02 s^{-1}; Table 4), whereas the rate of the N150F-catalyzed forward reaction (k_1 = 1.36 ± 0.03 s^{-1}; Table 4) is only 1.2-fold faster than that of the reverse reaction (k_2 = 1.12 ± 0.07 s^{-1}; Table 5). These results suggest that evolutionary pressure favored the selection of this invariant asparagine to endow ALAS with improved catalytic specificity toward the reaction with glycine and succinyl-CoA, while minimizing the reactivity with ALA.

We postulate that the selection of an amino acid with a polar, rather than a non-polar (particularly a phenyl group), side chain at position 150 of mALAS2 was influenced by the presence of the terminal carboxyl group in the acyl chain of succinyl-CoA. This deduction was reached from the observation that phenylalanine, in place of asparagine, is present in the glycine-rich stretch (or extended loop in CqsA) of AOS enzymes that utilize acyl-CoA substrates with hydrophobic acyl chains (acetyl-CoA in the case of KBL, palmitoyl-CoA in SPT, and decanoyl-CoA in CqsA) (17, 21, 22). In contrast, the polar amino acids histidine and asparagine are present in AONS (16) and ALAS, respec-

tively; these enzymes utilize acyl-CoAs whose acyl chains terminate with carboxyl groups (pimeloyl-CoA in the case of AONS).

However, additional evolutionary pressure(s) must have guided the selection of Asn-150 over other polar amino acids because, as demonstrated in our study, the N150H mutation has detrimental effects on the rate of the forward reaction. Thus, it is possible that during some evolutionary stage, besides the obvious positive selective pressure from the substrates, negative selective pressure by ALA also contributed to the shaping of the active site architecture of ALAS, culminating in the selection of Asn-150, which in turn was important in minimizing reactivity with ALA. This lack of reactivity was necessary to ensure that ALA is utilized predominantly for heme biosynthesis rather than for glycine and succinyl-CoA production. Moreover, Thr-148 (mALAS2 numbering), which resides on the Asn-150-containing glycine-rich stretch, has been shown to be essential for the specificity of ALAS toward the amino acid substrate (9, 10, 25). We conclude that the evolutionary selection of Thr-148 and Asn-150 contributed profoundly toward the functional specialization of ALAS, with the former amino acid helping the enzyme to differentiate itself from the other AOS enzymes in relation to substrate utilization, and the latter residue optimizing ALAS for ALA synthesis by favoring the forward reaction at the expense of the reverse.

Even though presently we cannot discern with certainty the molecular details that mediate the catalytic balance shift toward the reverse reaction, it is plausible that the N150H and N150F mutations decelerate the release of ALA from the active site, with the resulting accumulation and transformation of ALA into the quinonoid intermediate. This possibility is not without foundation if we consider that the analogous asparagine in *R. capsulatus* ALAS regulates the opening and closing of the alternative channel (Figs. 1 and 2 (a putative site for ALA release)) and that substitutions of Asn-150 reduce the k_{cat} values, which is at least partly determined by the rate of ALA release (11, 12). A different, but not mutually exclusive, possibility is that the active sites of the Asn-150 variants provide a catalytic environment that lowers the energetic barrier required for the chemical transformation of ALA into the quinonoid intermediate.

Author Contributions—B. M. S. and G. C. F. conceived and designed the project; B. M. S. acquired the data; B. M. S. and G. C. F. analyzed and interpreted the data; B. M. S. and G. C. F. wrote the paper. All authors reviewed the results and approved the final version of the manuscript.

References

1. Fratz, E. J., Stojanovski, B. M., and Ferreira, G. C. (2013) in *The Handbook of Porphyrin Science* (Ferreira, G. C., Kadish, K. M., Smith, K. M., and Guilard, R., eds) pp. 1–78, World Scientific Publishing Co., Singapore
2. Hunter, G. A., and Ferreira, G. C. (2011) Molecular enzymology of 5-aminolevulinate synthase, the gatekeeper of heme biosynthesis. *Biochim. Biophys. Acta* **1814,** 1467–1473
3. Eliot, A. C., and Kirsch, J. F. (2004) Pyridoxal phosphate enzymes: mechanistic, structural, and evolutionary considerations. *Annu. Rev. Biochem.* **73,** 383–415
4. Tan, D., and Ferreira, G. C. (1996) Active site of 5-aminolevulinate synthase resides at the subunit interface. Evidence from *in vivo* heterodimer formation. *Biochemistry* **35,** 8934–8941
5. Bottomley, S. S., and Fleming, M. D. (2013) in *The Handbook of Porphyrin Science* (Ferreira, G. C., Kadish, K. M., Smith, K. M., and Guilard, R., eds) pp. 44–87, World Scientific Publishing Co., Singapore
6. Whatley, S. D., Ducamp, S., Gouya, L., Grandchamp, B., Beaumont, C., Badminton, M. N., Elder, G. H., Holme, S. A., Anstey, A. V., Parker, M., Corrigall, A. V., Meissner, P. N., Hift, R. J., Marsden, J. T., Ma, Y., *et al.* (2008) C-terminal deletions in the ALAS2 gene lead to gain of function and cause X-linked dominant protoporphyria without anemia or iron overload. *Am. J. Hum. Genet.* **83,** 408–414
7. Balwani, M., Doheny, D., Bishop, D. F., Nazarenko, I., Yasuda, M., Dailey, H. A., Anderson, K. E., Bissell, D. M., Bloomer, J., Bonkovsky, H. L., Phillips, J. D., Liu, L., Desnick, R. J., and Porphyrias Consortium of the National Institutes of Health Rare Diseases Clinical Research Network (2013) Loss-of-function ferrochelatase and gain-of-function erythroid-specific 5-aminolevulinate synthase mutations causing erythropoietic protoporphyria and x-linked protoporphyria in North American patients reveal novel mutations and a high prevalence of X-linked protoporphyria. *Mol. Med.* **19,** 26–35
8. Nandi, D. L. (1978) Studies on δ-aminolevulinic acid synthase of *Rhodopseudomonas spheroides.* Reversibility of the reaction, kinetic, spectral, and other studies related to the mechanism of action. *J. Biol. Chem.* **253,** 8872–8877
9. Stojanovski, B. M., Hunter, G. A., Jahn, M., Jahn, D., and Ferreira, G. C. (2014) Unstable reaction intermediates and hysteresis during the catalytic cycle of 5-aminolevulinate synthase: implications from using pseudo and alternate substrates and a promiscuous enzyme variant. *J. Biol. Chem.* **289,** 22915–22925
10. Kaufholz, A. L., Hunter, G. A., Ferreira, G. C., Lendrihas, T., Hering, V., Layer, G., Jahn, M., and Jahn, D. (2013) Aminolaevulinic acid synthase of *Rhodobacter capsulatus*: high-resolution kinetic investigation of the structural basis for substrate binding and catalysis. *Biochem. J.* **451,** 205–216
11. Hunter, G. A., and Ferreira, G. C. (1999) Pre-steady-state reaction of 5-aminolevulinate synthase. Evidence for a rate-determining product release. *J. Biol. Chem.* **274,** 12222–12228
12. Zhang, J., and Ferreira, G. C. (2002) Transient state kinetic investigation of 5-aminolevulinate synthase reaction mechanism. *J. Biol. Chem.* **277,** 44660–44669
13. Hunter, G. A., Zhang, J., and Ferreira, G. C. (2007) Transient kinetic studies support refinements to the chemical and kinetic mechanisms of aminolevulinate synthase. *J. Biol. Chem.* **282,** 23025–23035
14. Hunter, G. A., and Ferreira, G. C. (1999) Lysine-313 of 5-aminolevulinate synthase acts as a general base during formation of the quinonoid reaction intermediates. *Biochemistry* **38,** 3711–3718
15. Mann, S., and Ploux, O. (2011) Pyridoxal-5′-phosphate-dependent enzymes involved in biotin biosynthesis: structure, reaction mechanism and inhibition. *Biochim. Biophys. Acta* **1814,** 1459–1466
16. Webster, S. P., Alexeev, D., Campopiano, D. J., Watt, R. M., Alexeeva, M., Sawyer, L., and Baxter, R. L. (2000) Mechanism of 8-amino-7-oxononanoate synthase: spectroscopic, kinetic, and crystallographic studies. *Biochemistry* **39,** 516–528
17. Ikushiro, H., and Hayashi, H. (2011) Mechanistic enzymology of serine palmitoyltransferase. *Biochim. Biophys. Acta* **1814,** 1474–1480
18. Ikushiro, H., Islam, M. M., Okamoto, A., Hoseki, J., Murakawa, T., Fujii, S., Miyahara, I., and Hayashi, H. (2009) Structural insights into the enzymatic mechanism of serine palmitoyltransferase from *Sphingobacterium multivorum*. *J. Biochem.* **146,** 549–562
19. Yard, B. A., Carter, L. G., Johnson, K. A., Overton, I. M., Dorward, M., Liu, H., McMahon, S. A., Oke, M., Puech, D., Barton, G. J., Naismith, J. H., and Campopiano, D. J. (2007) The structure of serine palmitoyltransferase; gateway to sphingolipid biosynthesis. *J. Mol. Biol.* **370,** 870–886
20. Han, G., Gupta, S. D., Gable, K., Niranjanakumari, S., Moitra, P., Eichler, F., Brown, R. H., Jr., Harmon, J. M., and Dunn, T. M. (2009) Identification of small subunits of mammalian serine palmitoyltransferase that confer distinct acyl-CoA substrate specificities. *Proc. Natl. Acad. Sci. U.S.A.* **106,** 8186–8191

21. Schmidt, A., Sivaraman, J., Li, Y., Larocque, R., Barbosa, J. A., Smith, C., Matte, A., Schrag, J. D., and Cygler, M. (2001) Three-dimensional structure of 2-amino-3-ketobutyrate CoA ligase from *Escherichia coli* complexed with a PLP-substrate intermediate: inferred reaction mechanism. *Biochemistry* **40,** 5151–5160
22. Jahan, N., Potter, J. A., Sheikh, M. A., Botting, C. H., Shirran, S. L., Westwood, N. J., and Taylor, G. L. (2009) Insights into the biosynthesis of the *Vibrio cholerae* major autoinducer CAI-1 from the crystal structure of the PLP-dependent enzyme CqsA. *J. Mol. Biol.* **392,** 763–773
23. Kelly, R. C., Bolitho, M. E., Higgins, D. A., Lu, W., Ng, W. L., Jeffrey, P. D., Rabinowitz, J. D., Semmelhack, M. F., Hughson, F. M., and Bassler, B. L. (2009) The *Vibrio cholerae* quorum-sensing autoinducer CAI-1: analysis of the biosynthetic enzyme CqsA. *Nat. Chem. Biol.* **5,** 891–895
24. Spirig, T., Tiaden, A., Kiefer, P., Buchrieser, C., Vorholt, J. A., and Hilbi, H. (2008) The *Legionella* autoinducer synthase LqsA produces an a-hydroxyketone signaling molecule. *J. Biol. Chem.* **283,** 18113–18123
25. Shoolingin-Jordan, P. M., Al-Daihan, S., Alexeev, D., Baxter, R. L., Bottomley, S. S., Kahari, I. D., Roy, I., Sarwar, M., Sawyer, L., and Wang, S. F. (2003) 5-Aminolevulinic acid synthase: mechanism, mutations and medicine. *Biochim. Biophys. Acta* **1647,** 361–366
26. Astner, I., Schulze, J. O., van den Heuvel, J., Jahn, D., Schubert, W. D., and Heinz, D. W. (2005) Crystal structure of 5-aminolevulinate synthase, the first enzyme of heme biosynthesis, and its link to XLSA in humans. *EMBO J.* **24,** 3166–3177
27. Reetz, M. T., Carballeira, J. D., Peyralans, J., Höbenreich, H., Maichele, A., and Vogel, A. (2006) Expanding the substrate scope of enzymes: combining mutations obtained by CASTing. *Chemistry* **12,** 6031–6038
28. Gong, J., and Ferreira, G. C. (1995) Aminolevulinate synthase: functionally important residues at a glycine loop, a putative pyridoxal phosphate cofactor-binding site. *Biochemistry* **34,** 1678–1685
29. Lendrihas, T., Hunter, G. A., and Ferreira, G. C. (2010) Targeting the active site gate to yield hyperactive variants of 5-aminolevulinate synthase. *J. Biol. Chem.* **285,** 13704–13711
30. Umanoff, H., Russell, C. S., and Cosloy, S. D. (1988) Availability of porphobilinogen controls appearance of porphobilinogen deaminase activity in *Escherichia coli* K-12. *J. Bacteriol.* **170,** 4969–4971
31. Ferreira, G. C., and Dailey, H. A. (1993) Expression of mammalian 5-aminolevulinate synthase in *Escherichia coli.* Overproduction, purification, and characterization. *J. Biol. Chem.* **268,** 584–590
32. Stojanovski, B. M., Breydo, L., Hunter, G. A., Uversky, V. N., and Ferreira, G. C. (2014) Catalytically active alkaline molten globular enzyme: effect of pH and temperature on the structural integrity of 5-aminolevulinate synthase. *Biochim. Biophys. Acta* **1844,** 2145–2154
33. Hunter, G. A., and Ferreira, G. C. (1995) A continuous spectrophotometric assay for 5-aminolevulinate synthase that utilizes substrate cycling. *Anal. Biochem.* **226,** 221–224
34. Gong, J., Hunter, G. A., and Ferreira, G. C. (1998) Aspartate-279 in aminolevulinate synthase affects enzyme catalysis through enhancing the function of the pyridoxal 5′-phosphate cofactor. *Biochemistry* **37,** 3509–3517
35. Lendrihas, T., Hunter, G. A., and Ferreira, G. C. (2010) Serine 254 enhances an induced fit mechanism in murine 5-aminolevulinate synthase. *J. Biol. Chem.* **285,** 3351–3359
36. Tan, D., Harrison, T., Hunter, G. A., and Ferreira, G. C. (1998) Role of arginine 439 in substrate binding of 5-aminolevulinate synthase. *Biochemistry* **37,** 1478–1484
37. Stojanovski, B. M., and Ferreira, G. C. (2015) Murine erythroid 5-aminolevulinate synthase: adenosyl-binding site Lys221 modulates substrate binding and catalysis. *FEBS Open Bio.* 10.1016/j.fob.2015.09.009
38. Johnson, K. A. (1992) in *The Enzymes* (Sigman, D. S, ed) pp. 1–61. Academic Press, New York